The drought risk of maize in the farming-pastoral ecotone in Northern China based on physical vulnerability assessment

Zhiqiang Wang[1,2], Jingyi Jiang[2,3], Qing Ma[4,5]

[1]National Disaster Reduction Center/Satellite Application Center for Disaster Reduction of the Ministry of Civil Affairs, Beijing 100124, China

[2]Key Laboratory of Disaster Reduction and Emergency Response, Ministry of Civil Affairs, Beijing 100124, China

[3]INRA-EMMAH UMR 1114, 84914 Avignon, France

[4]College of Geography, Beijing Normal University, Beijing 100875, China

[5]Chongqing No.18 High School, Chongqing 400020, China

Correspondence to: Jingyi Jiang (jiangjingyi1989@163.com)

Abstract. Climate change is affecting every aspect of human activities, especially the agriculture. In China, extreme drought events caused by climate change have posed great threaten to food safety. In this work we aimed to study the drought risk of maize in the farming-pastoral ecotone in Northern China based on physical vulnerability assessment. The physical vulnerability curve was constructed from the relationship between drought hazard intensity index and yield loss rate. The risk assessment of agricultural drought was conducted from the drought hazard intensity index and physical vulnerability curve. The probability distribution of drought hazard intensity index decreased from southwest to northeast and increased from southeast to northwest alone the rainfall isoline. The physical vulnerability curve had a reduction effect in three parts of farming-pastoral ecotone in Northern China which helped to reduce drought hazard vulnerability on spring maize. The risk of yield loss ratio calculated based on physical vulnerability curve was lower compared with the drought hazard intensity index which suggested that the increasing capacity of spring maize to resist drought and adapt to drought.In conclusion, the farming-pastoral ecotone in Northern China had great sensitivity to climate change and high probability for severe drought hazard. Risk assessment of physical vulnerability can help better understanding the physical vulnerability to agricultural drought and can also promote measurements to adapt to the climate change.

1 Introduction

Climate change and its influence on human activity have gained more and more attention from different fields and communities. In the past 30 years, the global surface temperature kept the linear growth trend and the frequency and intensity of extreme climate events increased (IPCC, 2014). Even though many measures have been taken to tackling climate change, the tendency will keep in the next period of time. In arid areas, water shortage resulted from climate change during the crop growing stage will lead to loss of yield, increase the frequency of agricultural drought and threaten the food security (FAO, 2013;Wheeler and von Braun, 2013). In Africa, climate change will amplify existing stress on water availability and agricultural systems particularly in semi-arid environments. In Asia, agricultural productivity will be declined because of the climate change in many sub-regions for crops like rice (IPCC, 2014). For China, drought is one of the most obvious performances of climate change (Piao et al., 2010). In the past 60 years, China has suffered a number of severe drought hazards which caused great loss of agricultural production (Zou et al., 2005). Hazard is called a dangerous phenomenon, substance, human activity or condition that may cause loss of life, injury or other health impacts, property damage, loss of livelihoods and services, social and economic disruption, or environmental damage (UNISDR, 2009). Better understanding and evaluation of agricultural drought hazard can help people raise the capacity of responding to agricultural drought hazard and put forward countermeasures to reduce risk of agricultural drought hazard in high-risk areas.

Risk is defined as the combination of the probability of an event and its negative consequences (UNISDR, 2009). As the core of disaster risk assessment, study about vulnerability has been widely applied in many different fields like ecology, public health and global climate change (Füssel, 2007). Initially, vulnerability was defined as the human response to hazard events (Blaikie and Cannon, 1994;FAO, 2001). Gradually, vulnerability is added with some new meanings including the different systems of human society responding to hazard, the interaction process of multi-factors like nature, society, economy and environment (UNDP, 2004) , the sensitivity or susceptibility to hazards and the capacity to cope and adapt to hazards (IPCC, 2014). Many methods have been proposed to assess vulnerability. Statistical method builds the relationship between impact factors and vulnerability to reflect the characteristic of vulnerability (Simelton et al., 2009). But this method cannot consider different kinds of factors synthetically. Another kinds of methods like fuzzy modeling and

multi-indicator method (Antwi-Agyei et al., 2012;Kim et al., 2015) can provide a compressive assessment for different impact factors. But fuzzy modeling method is restricted by background knowledge and information. So it is hard to set weight for different indicators. For multi-indicator method, some information will be dropped during the process of integrating different indicators. Cluster analysis method can consider different impact factors separately and determine the most vulnerable places based on different combinations of the components of vulnerability (Sharma and Patwardhan, 2008). The advantage of this method is its ability to maintain information from different factors completely. Compared with fuzzy modeling and multi-indicator method, it can provide richer information for decision makers. But this method is always restricted to qualitative description of vulnerability and cannot quantitatively describe the vulnerability of hazard-affected body.

However, all those studies discussed above did not consider physical factors and social factors separately. This will cause great restrict to realize the mechanism of disaster from its formation process. Different from the system vulnerability caused by social factors, physical vulnerability is an internal characteristic of hazard-affected body. It is the capacity of hazard-affected body to response, resist and recover from strike caused by nature or human beings (Wang et al., 2013a). Many studies have quantitatively analyzed the physical vulnerability of different disasters: Uzielli et al. (2008) utilized the relationship between landslide intensity and the susceptibility of vulnerable elements to quantitatively estimate physical vulnerability of the built environment and population to landslides. Douglas (2007) used fragility curves to model physical vulnerability for evaluation of earthquake and landslide risk. For physical vulnerability of agricultural drought hazard, most studies chosen geographical statistical methods or different drought index with meteorology, hydrology or remote sensing data to calculate the distribution of drought hazard risk (Kellner and Niyogi, 2014;Karavitis et al., 2014;Jain et al., 2015;Murthy et al., 2015). But all these studies did not consider the relationship between meteorological factors and crop water stress during the process of crop growth, so it is hard to determine the physical vulnerability of crop to drought hazard. Based on the crop growth model, Wang et al. proposed a Hazard–Loss curve to construct the relationship between drought hazard intensity and crop yield loss and utilized the curve to simulate the physical vulnerability of hazard-affected crop with environmental policy-integrated climate (EPIC) model. As the drought hazard intensity is calculated from the accumulation of crop daily water stress, so the physical vulnerability curve can better reflect the biophysics regulation during crop growth and avoid errors caused by the integration of multi-parameters. Physical vulnerability curve makes the drought

hazard vulnerability become a parameter which can be described quantitatively in a dynamic process and provides the probability to assess physical vulnerability of agricultural drought hazard from the aspect of disaster mechanism.

To construct physical vulnerability curve, the key point is to calculate the drought hazard intensity index and the corresponded crop yield loss ratio. In previous study (Wang et al., 2015)，a new method was proposed to determine drought hazard intensity index based on the daily water stress from EPIC model and yield loss contribution rates for different growth stages. In this study, the risk assessment of agricultural drought was conducted from the physical vulnerability curve. Firstly, under the circumstances of no irrigation, the drought hazard intensity index was calculated from the daily water stress and yield loss contribution rates for different growth stages. Based on the distribution of drought hazard intensity index, the risk of drought hazard intensity index in different regions was analyzed. Then, the yield loss ratio was got from the difference of yield with two different scenarios (sufficient irrigation and no irrigation). With the spatial distribution of drought hazard intensity index, sites with different drought hazard intensity index and yield loss ratio were selected. A Logistc model was used to simulate the physical vulnerability curve of crop from the relationship between hazard and loss. According to the physical vulnerability curve, both the physical vulnerability assessment and risk assessment of yield loss ratio were analyzed.

Ecotone is defined as a multi-dimensional environmentally interaction zone between ecological systems (Hufkens et al., 2009). Because of its sensitivity to climatic variation, environmental change and human activity, ecotone tends to shift in space and time over several spatial scales (Kark, 2013). For example, the African Sahel is regarded as a typical ecotone, which is influenced by fluctuations in climate and human activities (Herrmann et al., 2005;Rian et al., 2009). In East Asia, the farming-pastoral ecotone in Northern China stretching across the monsoon fringe area from southwest to northeast are dominated by adjacent ecological systems of steppes and crops (Lu and Jia, 2013). As the typical ecotone with the largest area and longest span in the world, the farming-pastoral ecotone in Northern China is highly sensitive to climate change in East Asia. Many researchers utilized historical meteorological data including temperature, precipitation and remote sensing data to compositely analyze the impacts of climate change and socioeconomic factors on boundary shifts and land use change of the farming-pastoral ecotone in Northern China (Liu et al., 2011;Ye and Fang, 2013;Geng et al., 2014;Shi et al., 2014). Results show that the extent of the farming-pastoral ecotone in Northern China greatly

fluctuated in accordance with the variability of precipitation (Lu and Jia, 2013;Geng et al., 2014). Meanwhile, the dry climate conditions and long-term excessive human activity have made desertification in this region a serious environmental problem that affects the economy and society development (Xu et al., 2014). Based on the simulation from land use scenario dynamic model, it is predicted that the farming-pastoral ecotone in northern China will become increasingly vulnerable and hotspots for land-use change with the intensified drying trends (Geng et al., 2014). So the farming-pastoral ecotone in Northern China was chosen as the study area in this study. In addition, as the spring maize, which is a kind of drought-resistant crops, is widely planted in this region, so spring maize was selected as a typical crop for the risk assessment of physical vulnerability in the farming-pastoral ecotone in Northern China. The assessment results showed the farming-pastoral ecotone in Northern China is a region with high risk of agricultural drought. To better adapt to drought, more attentions should be paid in this region and more methods like changing the growth environment of crop to reduce the strength of drought hazard intensity index, developing improved varieties of crops to reduce physical vulnerability of agricultural drought and reducing crop's exposure to drought during the planting process should be adopted to responses to climate change.

2 Data and methodology

2.1 Study area and data

2.1.1 Study area

The farming-pastoral ecotone in Northern China is sensitive to climate change and belongs to rain-fed agriculture region which is fragile in ecology, agriculture drought hazard risk assessment of this region. It can reflect the time-spatial variation of drought hazard resulted from climate change. There exist many different definitions about the farming-pastoral ecotone in northern China. In general, it is located at the north part of China with the rainfall isoline changing from 300mm to 400mm, annual precipitation change ranging from 15% to 30% and dryness changing from 1.0 to 2.0 (Zhao et al., 2002). The precipitation period is between June and August with large interannual variation. According to the distribution of landform and vegetation zonality, the farming-pastoral ecotone in northern China can be classified into three parts: the east part, the middle part and the west part. The east part is the transition area of Northeast China Plain and Inner Mongolian Plateau with vegetation types changing from warm

temperate deciduous forests to temperate forest steppe. The annual average temperature is from 3 to 7℃.The middle part transits from North China Plain to Loess Plateau with the vegetation changing from warm temperate deciduous forests to temperate grassland. Because of the relatively high altitude, the annual average temperature here is from 0 to 1℃. The west part is the transition area from Loess Plateau to Qinghai-Tibet Plateau with the vegetation changing from warm temperate deciduous forests to temperate desert steppe. The annual average temperature is from 6 to 9℃. Fig. 1 shows the location and the land-use of the farming-pastoral ecotone in Northern China. The east part, middle part and west part of the farming-pastoral ecotone in Northern China are located from east to west respectively. The blue triangles represent 54 meteorological stations covering the whole region and the yellow regions are cultivated land. Different shades of black lines show the change of rainfall isolines, which increase from northwest to southeast and extension alone the direction of northeast to southwest.

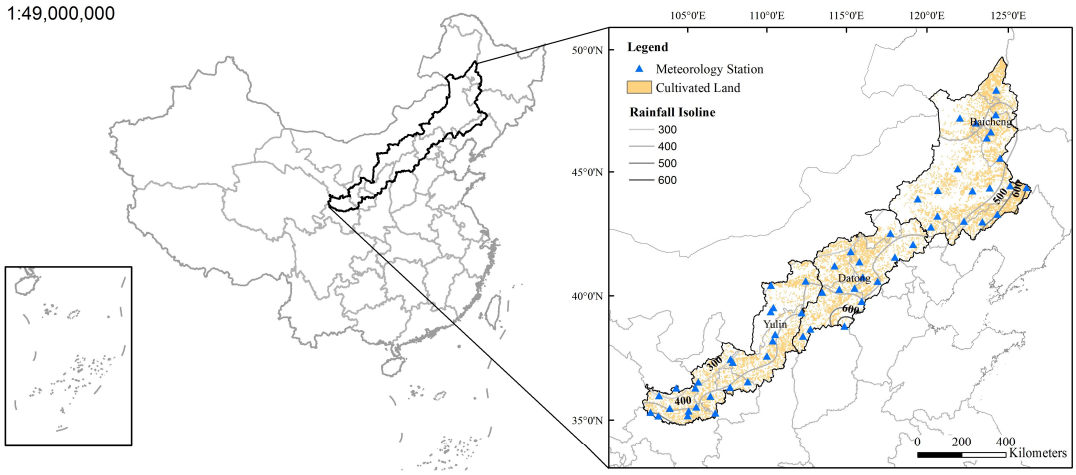

Figure 1: Location and the land-use map of the farming-pastoral ecotone in Northern China

2.1.2 Data

The data used in this study include meteorological data of the farming-pastoral ecotone in Northern China from 1966 to 2011, soil data and the agricultural data (Table 1). The daily meteorological data came from 54 meteorological stations of the study area. Daily solar radiation information was recorded in 27 stations. The daily solar radiation data for the remaining stations were estimated based on the sunshine duration data using the Angstrom-Prescott model (Angstrom, 1924;Prescott, 1940). The soil texture data were retrieved from ‘‘Chinese Soil Genus Records’’ and transformed into the USDA soil-type system (Skaggs et al., 2001).

Table 1: Meteorological, soil and relative agricultural data

Database	Content	Source
Meteorological data	Daily data from 1960 to 2011: precipitation, temperature, radiation, wind speed and relative humidity et al.	China meteorological data sharing service system of China Meteorological administration
Spatial distribution of soil	1:1,000,000 soil map of the study area	Institute of Soil Science, Chinese Academy Sciences
Soil properties	Soil layers, texture data and organic carbon and so on	Chinese Soil Genus Records
Land use map	Land use map of the study area in 2000. The main land use type including paddy field, dry land, forest land, grass land and so on.	Institute of Remote Sensing and Digital Earth Chinese Academy of Sciences
Statistical agricultural data	Fertilization, sowing area, yields from 1966 to 2011.	China Statistical Yearbook

2.2 Methodology

The process of assessment is shown in Fig. 2. As the disaster risk (R) are the function of hazard factor (H), physical vulnerability (V), exposure (E) and the disaster reduction capacity of hazard-affected body to hazard (C_H), physical vulnerability (C_V) and exposure (C_E) (Eq. 1), so under the assumption that all maize was exposed to drought hazard, both hazard intensity index and the physical vulnerability curve was simulated through EPIC model to assess the risk of spring maize in the farming-pastoral ecotone in Northern China.

$$\mathrm{R} = \frac{H \times V \times E}{C_H \times C_V \times C_E} \tag{1}$$

The station EPIC model was used to calibrate the genetic parameter of local maize. Then a water-deficit experiment on different growth stage was conducted to calculate the yield loss contribution rate. So the maize drought hazard intensity index was defined based on daily water stress and the yield loss contribution rate. Added with the spatial data in time series, the spatial EPIC model was used to calculate the spatial maize drought hazard intensity index. Meanwhile, the yield loss ratio was got from the difference of yield under two different simulated scenarios with EPIC model (One was sufficient irrigation and the other one was no irrigation). After this, the physical vulnerability curve was constructed from sites under different drought hazard intensity using Logistic regression model to describe the relationship between drought hazard and yield loss. According to the function of disaster risk, the risk assessment of drought hazard was conducted from three aspects: the first was the risk assessment of drought hazard intensity index; the second was physical vulnerability assessment of spring

maize based on physical vulnerability curve; the third one was the risk assessment of yield loss ratio calculated from physical vulnerability curve.

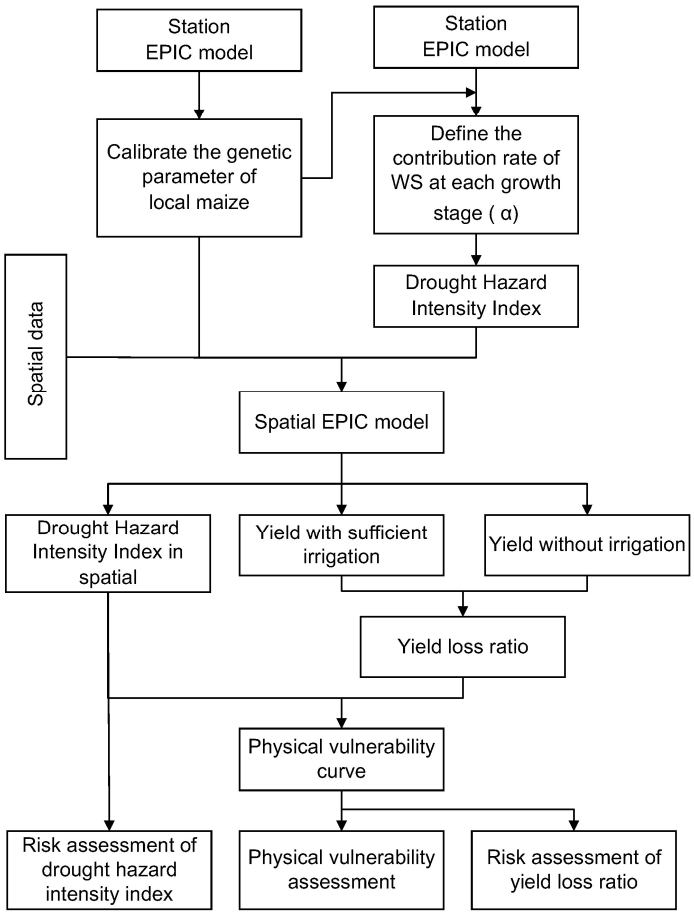

Figure 2: Flow chat of drought risk based on physical vulnerability assessment

2.2.1 Drought Hazard Intensity Index

EPIC model is a field-scale crop model, which is capable of simulating daily crop growth, calculating crop yield under various climate and environment conditions and performing long-term simulations for hundreds of years (Gassman et al., 2005). In recent years, EPIC model has been applied in different fields, including climate change (Izaurralde et al., 2012;Rinaldi and De Luca, 2012), simulation of crop yields (Pumijumnong and Arunrat, 2013;Xiong et al., 2014) and drought disaster risk assessment (Jia et al., 2012;Wang et al., 2013b). For different kinds of crop, genetic parameters used in EPIC model vary with different varieties and geographical conditions. So before the simulation with EPIC model, it is necessary to localize the genetic parameter of crops based on the field measurements. In addition, parameters like soil parameters, filed management parameters and daily meteorological data are also input parameters to

run EPIC model.

According to the three parts of the farming-pastoral ecotone in Northern China defined in the last section, we chose three represent stations (east part: Baicheng, middle part: Datong, west part: Yulin) to calculate genetic parameters of spring maize of each part. In each station, the annual yields of spring maize from 2000 to 2005 from agriculture statistic yearbooks were selected as the recorded yields to adjust the genetic parameters. In addition, the daily meteorological data from 2000 to 2005, the soil data and the field management data were all put into the station EPIC model. The genetic parameters such as energy biomass conversion factor, harvest index were finally determined after a number of adjustments based on the comparison between the model output crop yields and the recorded data. The simulation results of spring maize for each station are demonstrated in Fig. 3. To validate the accuracy of the determined genetic parameters, the annual yields from agriculture statistic yearbooks in another 6 stations (Chifeng, Tongliao, Zhangjiakou, Jining, Guyuan and Dingxi) within the study area from 2000 to 2005 were selected. Fig. 4 shows the validation result between the simulated results and the recorded yields. The correlation coefficient R^2 is 0.86. Seen from the validation result, the determined genetic parameters of spring maize were appropriable for this study. For the difference between simulated results and recorded data, errors mainly came from the input data of station EPIC model including daily meteorological data and yield management data.

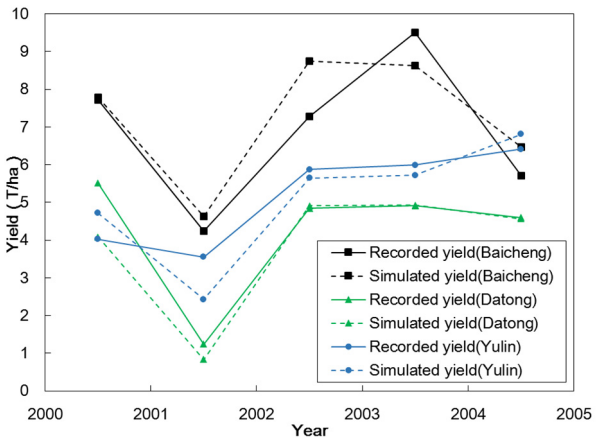

Figure 3: Calibration of the genetic parameters using the recorded yields of spring maize at Baicheng, Datong, Yulin station.

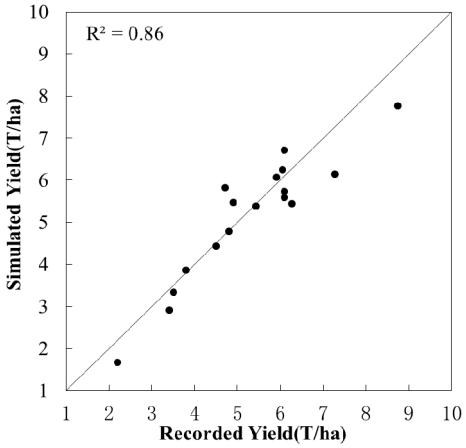

Figure 4: Validation of the genetic parameters using the recorded yields of spring maize at six stations in the study area from 2000 to 2005.

After running the EPIC model, parameters which describe the growth state of crops are output. Among them, water stress, which can reflect the relationship between water supply and demand during the crop growth process, is an important parameter in risk assessment of agricultural drought. So during

the calculation of drought hazard intensity index, water stress is selected as the main factor to describe the intensity of drought. In addition, because water stress will have different influence on crop yield in different crop growing stage, so the yield loss contribution rate of water stress (α) (Wang et al., 2015), which is calculated from the proportion of yield reduction rate in each stage to the summary of the yield reduction rate in different stages (Eq. 2), is also used to reflect water critical period for crop yields. *m* stages of crop growth are defined based on crop growth regulation.

$$\alpha_i = \frac{y_i}{\sum_{i=1}^{m} y_i} \tag{2}$$

where $y_i=Y_i/Ys$, *Ys* is the yield under the situation of sufficient soil water supply and *Yi* is the yield under water shortage in growth stage *i*. m is the number of growth stages.

Based on the EPIC water stress and the calculated yield loss contribution rate, the equation of drought hazard intensity index is as follows (Wang et al., 2015):

$$DHI_{yj} = \frac{\sum_{k=1}^{n} \alpha_i (1 - WS_k)}{\max DHI} \tag{3}$$

where DHI_{yj} is the drought hazard intensity index of y year in unit *j*; WS_k is the water stress on day *k*; α_i is the yield loss contribution rate of WS_k and *k* belongs to the *i* growth stage; *n* is the total days when there is water stress; max *DHI* denotes the maximum value of $\sum_{k=1}^{n} \alpha_i (1 - WS_k)$ in all the simulated years and units. DHI_{yj} varies from 0 (0 represents the minimum intensity of drought hazard) to 1(1 represents the maximum intensity of drought hazard).

2.2.2 The establishment of physical vulnerability curve

To determine the impact of water stress on crop yields, both the crop genetic parameters and daily meteorological data after spatial interpolation are put into the spatial EPIC model. With the guarantee of soil nutrient and ventilation, two scenarios (*Y1*: sufficient irrigation; *Y2*: no irrigation) are set to simulate the growth of the crop. For each unit, the difference of crop yields between two scenarios for each year is the year yield loss under water stress. So the proportion between the year yield loss and the maximum yield with sufficient irrigation for multi-years in this unit is defined as the yield loss ratio under water stress (Wang et al., 2013a):

$$YL_{yj} = \frac{Y1_y - Y2_y}{\max Y1_j} \tag{4}$$

where YL_{yj} is the loss rate of yield of y year in station j; $Y1_y$ and $Y2_y$ are the unit yield of y year under scenario $Y1$ and $Y2$; max $Y1_y$ represents maximum unit yield of station j.

Based on drought hazard intensity index and the corresponded yield loss rate, the physical vulnerability curve is defined to simulate the relationship between them using the regression analysis method. For each kind of crop, the physical vulnerability curve is an internal property for hazard-affected body itself. The key point to establish the physical vulnerability curve is to set up a wide range of sceneries from no drought to extreme drought hazard. The more scenarios of drought hazard intensities are included, the more accurate physical vulnerability curve will be got. So in this study, according to the drought hazard intensity index we calculated from different evaluation units in different years, we try to select more sites under different sceneries of drought hazard intensities. And then the Logistic regression analysis is used to simulate the physical vulnerability curve of the crop from selected points.

2.2.3 Risk assessment of agricultural drought

In this study, drought hazard intensity index and physical vulnerability curve are two cores of the drought risk assessment. Based on the formulation process of agricultural drought hazard, the risk assessment of drought hazard intensity index, the physical vulnerability assessment on spring maize and the risk assessment of yield loss ratio calculated from physical vulnerability curve were conducted sequentially. For drought hazard intensity index, as it is calculated from crop daily water stress and yield loss contribution rate, it can reflect the degree of agricultural drought on specific crop. So the time series, standard deviation and slope of drought hazard intensity index on each evaluation unit were calculated to analyze the spatial-temporal distribution of agricultural drought. The probability distribution of drought hazard intensity index was processed for the risk assessment. For physical vulnerability assessment, it was conducted relying on physical vulnerability curve of spring maize. For the yield loss ratio calculated from physical vulnerability curve, as it is determined by both drought hazard intensity index and the corresponded physical vulnerability, so the calculated yield loss ratio is a good representative of drought risk. The standard deviation, slope and probability of yield loss ratio were calculated to show the spatial-temporal distribution and probability distribution of drought risk.

3 Results

3.1 Risk assessment of maize drought hazard intensity index

Based on the classification method of annual crop climate types (AQSIQ/SAC, 2008), year 2002 was selected as the climate normal year to calculate the yield loss contribution rates of water stress at Baicheng, Datong and Yulin with the corresponded genetic parameters of the spring maize. According to the growth regulation of spring maize, six growth stages were determined in Table 2. With the crop yield under sufficient irrigation as the comparison, the water-deficit treatment in each growth stage was conducted respectively with station EPIC model. The resulted yield losses were recorded. According to Eq. 2, the yield loss contribution rates in different growth stages for each station were shown in Table 2. For more details about the experiment of water-deficit, Wang et al. (2015) is referenced.

Table 2: Yield loss contribution rate α at Baicheng, Datong and Yulin.

		Growth stage of spring maize						
		Seeding stage	Jointing stage	Early heading stage	Late heading stage	Early grain-filling stage	Late grain-filling stage	Mature stage
Yield loss contribution Rate α_i	Baicheng	0.17	0.22	0.18	0.18	0.16	0.09	0
	Datong	0.16	0.25	0.19	0.16	0.15	0.08	0
	Yulin	0.17	0.18	0.22	0.17	0.16	0.10	0

We used the genetic parameters and yield loss contribution rates got from three sites to represent genetic parameters and yield loss contribution rates in the east, middle and west part of the farming-pastoral ecotone in Northern China respectively. With the evaluation unit of 5km×5km area, the interpolated meteorological data from 1966 to 2011 and the genetic parameters for each part were put into the spatial EPIC model. Under the situation of no irrigation, the daily water stress of each evaluation unit in study area was output. Based on Eq. 3, the spatial distribution of drought hazard intensity index of the farming-pastoral ecotone in Northern China was calculated finally.

Fig. 5 shows the distribution of spring maize drought hazard intensity index in the farming-pastoral ecotone in Northern China in every five year. For most years, the drought hazard intensity index of spring maize increased from northeast (0.1) to southwest (0.5) and decreased back to 0.1 at the margin of southwest. Compared with the rainfall isoline, there existed a negative correlation between the drought hazard intensity index and precipitation. For regions with the rainfall isoline lower than 300mm, drought

hazard intensity index for most years were around 0.5 or 0.6. But with the rise of precipitation, drought hazard intensity index declined gradually. For regions with rainfall isoline from 500mm to 600mm, most drought hazard intensity indexes centered on 0.1. In generally, the middle part and most region of the west part were the driest part of the whole study area with the average of drought hazard intensity index for multi-years larger than 0.5.

Seen from the time series of drought hazard intensity index in the farming-pastoral ecotone in Northern China, there existed two extreme drought hazards in 1980 and 2000 with the average of drought hazard intensity index larger than 0.8. For other years, areas with the drought hazard intensity index larger than 0.5 mainly centered in the west part. A cyclic behavior with a return period of 20 years aprox appears from 1965 to 2000. Since 2005, regions with the drought hazard intensity index larger than 0.5 spread toward northeast. In 2010, except little areas, the drought hazard intensity index for the whole study ranged from 0.4 to 0.6.

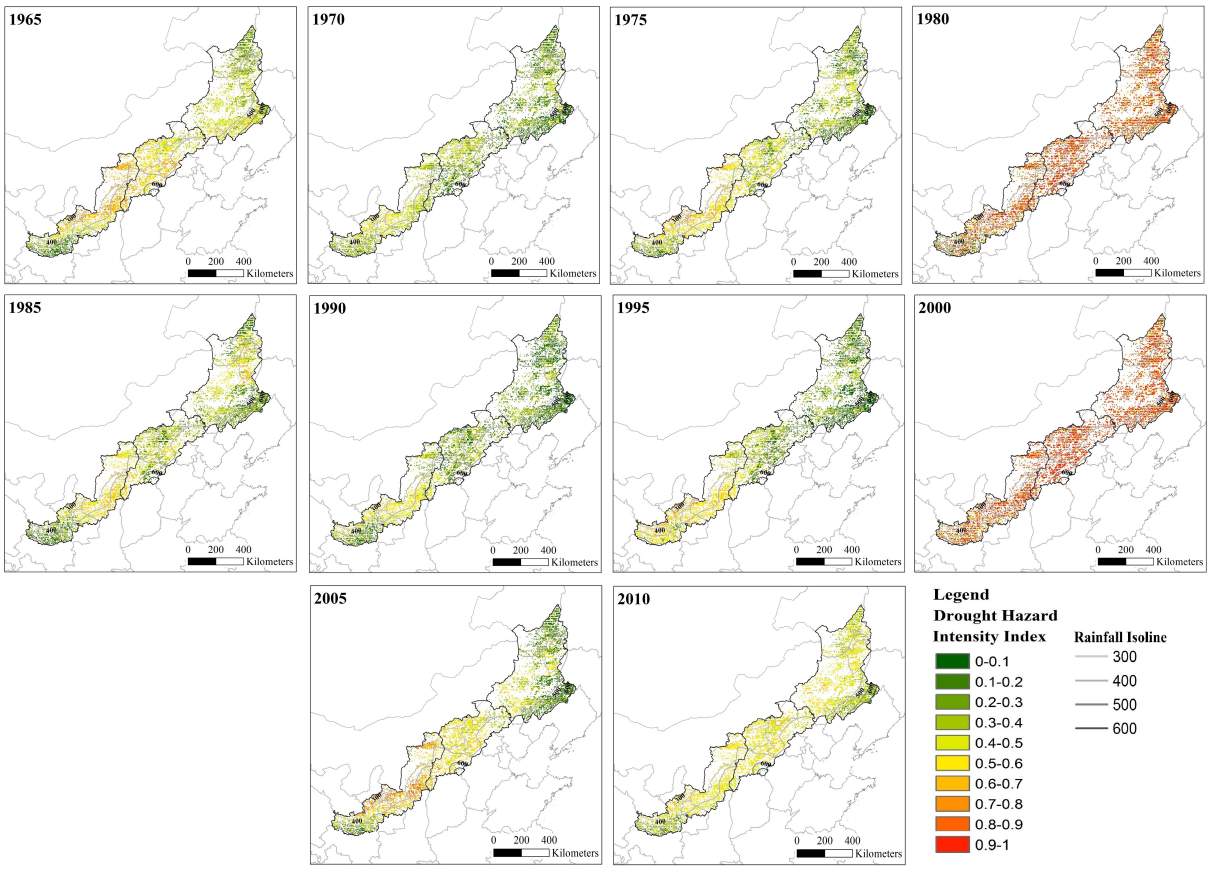

Figure 5: The spatial distribution of spring maize drought hazard intensity index in time series.

To reveal the fluctuation of drought hazard intensity index of spring maize in time series, the standard deviation from 1966 to 2011 of each evaluation unit in the study area was calculated. Fig. 6 is

the distribution of standard deviation of spring maize drought hazard intensity index from 1966 to 2011. For most parts, the standard deviation was from 0.1 to 0.3 and had the tendency of decreasing from northeast to southwest. The east part had the highest standard deviation (0.3), which showed greatest interannual fluctuation of spring maize drought hazard intensity index. But the standard deviation in west part ranging from 0.1 to 0.2 was relatively low.

In order to describe the variation tendency of drought hazard intensity index from 1966 to 2011 in the farming-pastoral ecotone in Northern China, the slope of linear regression of drought hazard intensity index for 46 years were calculated. Fig. 7 is the distribution of slope of spring maize drought hazard intensity index from 1966 to 2011. Warm-toned colors like red and yellow represent slope larger than 0 and the increasing tendency of drought hazard intensity index, while cool-toned colors like green represent slope smaller than 0 and the decreasing tendency of drought hazard intensity index. For the whole farming-pastoral ecotone in Northern China, the change of slope was small ranging from -0.006 to 0.006. But for the most parts, the slope was larger than 0, which meant the intensity of drought hazard strengthened. The middle part had the most obvious increasing tendency (from 0.002 to 0.006).The next was east part within the rainfall isoline from 300mm to 400mm and little region at the southwest edge of the study area with the slop changing from 0.002 to 0.004.

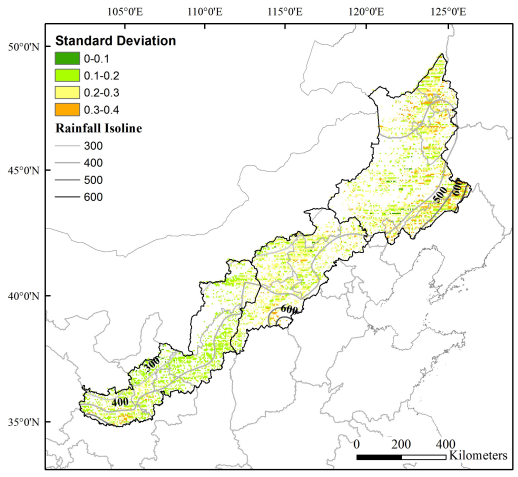

Figure 6: Standard deviation of spring maize drought hazard intensity index from 1966 to 2011.

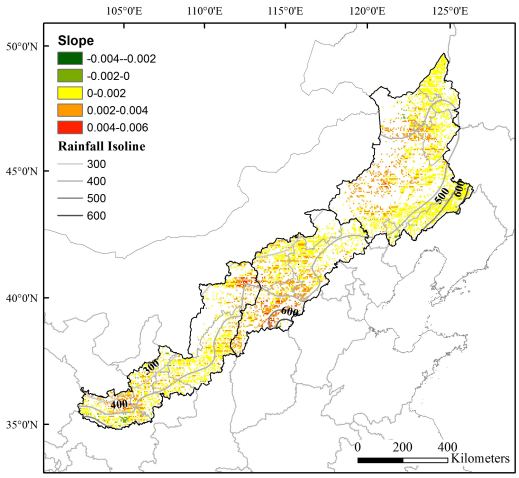

Figure 7: Slope of linear regression of spring maize drought hazard intensity index from 1966 to 2011.

To access the risk of spring maize drought hazard intensity index in the farming-pastoral ecotone in Northern China, we calculated the exceeded probability of spring maize drought hazard intensity index for each evaluation unit. Through fixing the drought hazard intensity index, probability distribution of spring maize drought hazard intensity index with 4 hazard levels was drawn separately: spring maize

drought hazard intensity index≥0.2 (Fig. 8(a)), spring maize drought hazard intensity index≥0.3 (Fig. 8(b)), spring maize drought hazard intensity index≥0.4 (Fig. 8(c)) and spring maize drought hazard intensity index≥0.5 (Fig. 8(d)).

Seen from Fig. 8, the high value area of the probability was located at most region of west part and middle part, while the low value area was located at the east part within the rainfall isoline from 500mm to 600mm and the southwest edge of the west part. For most region of west part, the upper limit of probability was 1 under four hazard levels. So there existed very high probability of drought hazard and would encounter big disaster losses almost every year. For the middle part, the upper limit of probability under 4 hazard levels from 0.2 to 0.5 was 1, 1, 0.8 and 0.5 respectively. So in this region, drought hazard with the intensity index of 0.2 and 0.3 would occur nearly every year. The risk level of drought hazard with the intensity index of 0.5 was every two years. For these two low value regions, the upper limit of probability under 4 hazard levels from 0.2 to 0.5 was 1, 0.9, 0.4 and 0.2 respectively. These regions would meet the drought hazard with the intensity index of 0.2 every year and the risk level of drought hazard with the intensity index of 0.5 was at least every five years.

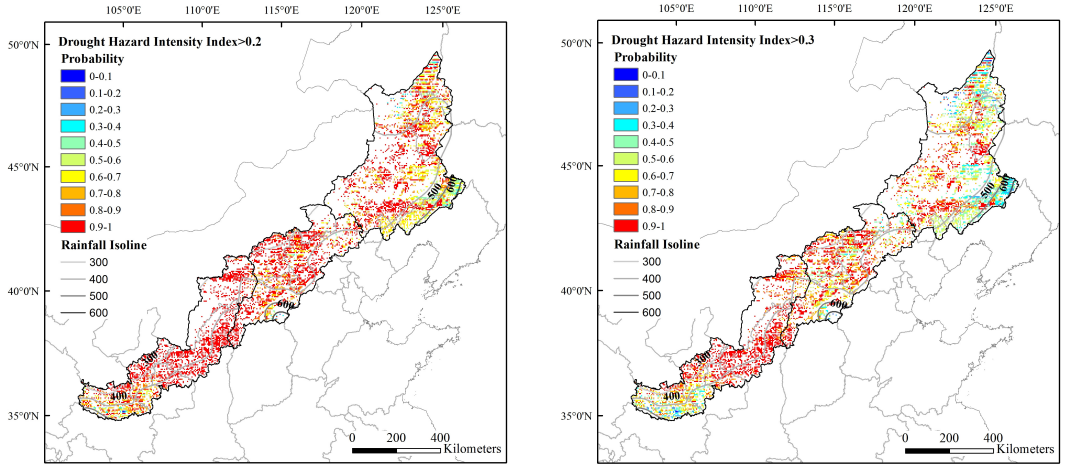

(a) (b)

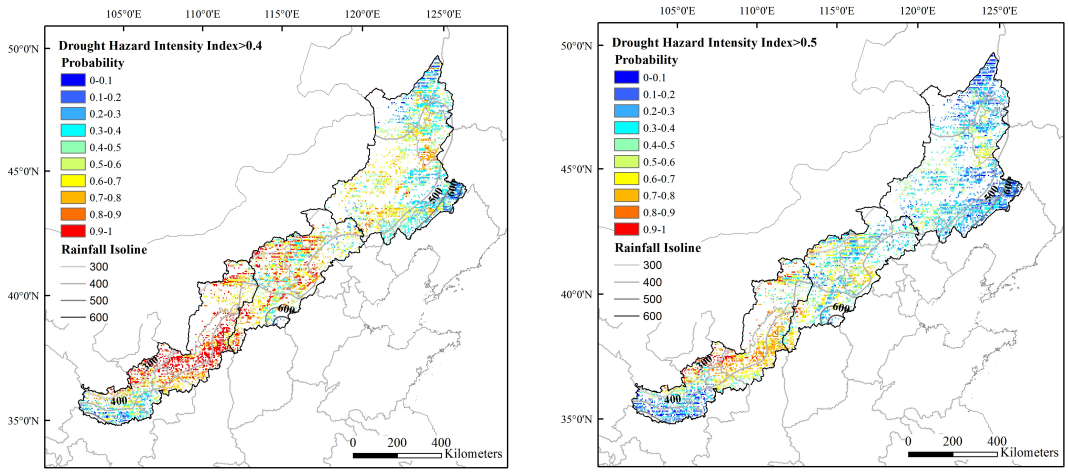

(c) (d)

Figure 8: Probability distribution of spring maize drought hazard intensity index for different hazard levels. (a) Drought hazard intensity index≥0.2; (b) Drought hazard intensity index≥0.3; (c) Drought hazard intensity index≥0.4; (d) Drought hazard intensity index≥0.5.

3.2 Physical vulnerability curve of spring maize

Based on the genetic parameters of spring maize for three parts of farming-pastoral ecotone in Northern China, the spatial EPIC model was conducted under two scenarios (*Y1*: sufficient irrigation; *Y2*: no irrigation). For each evaluation unit, the loss rate of yield was got according to Eq. 4. Combined with the spatial distribution of drought hazard intensity index, 50 sites under different drought hazard intensity were selected for each part to extract drought hazard intensity index and the corresponded loss rate of yield for 46 years. For each part of the farming-pastoral ecotone in Northern China, a scatter diagram which describes the drought hazard intensity curve-yield loss rate is shown in Fig. 9. Each point represents the annual loss rate of yield and drought hazard intensity for a given site. The solid line is the physical vulnerability curve simulated using logistic curve fitting methodology. For each part, the physical vulnerability of spring maize could be evaluated using the physical vulnerability curve as follows:

$$Y_e = \frac{0.57}{(1+8.81e^{-6.33H_e})} \tag{5}$$

$$Y_m = \frac{0.58}{(1+11.49e^{-8.9H_m})} \tag{6}$$

$$Y_w = \frac{0.54}{(1+10.821e^{-7.68H_w})} \tag{7}$$

where Y_e, Y_m and Y_w represent the yield loss ratios of spring maize in east, middle and west parts and H_e,

H_m and H_w are the drought hazard intensity indexes in east, middle and west parts. R^2 is 0.70 for east part, 0.71 for middle part and 0.65 for west part.

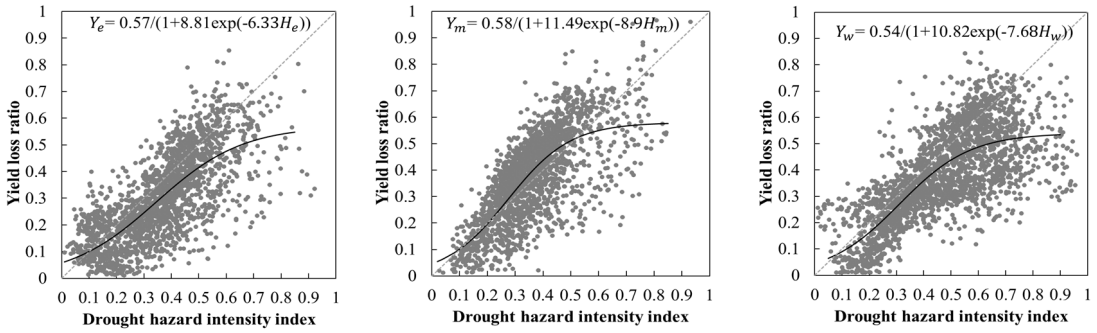

Figure 9: Physical vulnerability curve to drought hazard of spring maize at (a) east part (b) middle part and (c) west part of the farming-pastoral ecotone in Northern China.

Restricted by the meteorological data, it was hard to include every different meteorological scenery in theoretical like extreme drought (H = 1) or no drought (H = 0) to simulate a real physical vulnerability curve to drought hazard of spring maize. In addition, errors from meteorological data and the model itself might also have impacts on simulation results. So considering the accuracy of the input data and some uncertainties during the calculation process, the simulated drought physical vulnerability curve of spring maize for each part was satisfied in this study.

Comparing three different kinds of spring maize planted in the study area, the physical vulnerability curve of spring maize for each part is slightly different from each other. But as these three regions are adjacent and are all located at the farming-pastoral ecotone in Northern China which is relatively drought, the difference is not obvious. For each curve, at the beginning stage, the yield loss ratio is mild with low drought hazard intensity index (0 to 0.2). Then the increase of yield loss ratio is swift with middle drought hazard intensity index (0.2 to 0.6). For the last stage, the yield loss ratio reaches the highest point and becomes stable with high drought hazard intensity index (0.6 to 1). For each part of the study area, all of these curves are below or near 1:1 line, which show reduction-effect of drought hazard intensity and the reduction of drought hazard vulnerability on spring maize.

3.3 Risk assessment of yield loss ratio based on physical vulnerability curve

We assumed that the spring maize in the study area was completely exposed to drought hazard, so the drought risk of spring maize is mainly determined by the drought hazard intensity index and its

vulnerability under this drought hazard intensity. So in this section, we put the calculated drought hazard intensity index of each evaluation unit into the physical vulnerability curve to get the simulated yield loss ratio. The risk assessment was conducted on the basis of the distribution of yield loss ratio for each unit.

To describe the change of yield loss ratio in time series, both the standard deviation and the slope of yield loss ratio from 1966 to 2011 were calculated on each evaluation unit. Fig. 10 is the distribution of standard deviation of yield loss ratio in farming-pastoral ecotone in Northern China. Similar with the standard deviation of drought hazard intensity index, the standard deviation of yield loss ratio also showed the tendency of decline from northeast to southwest. But because of the reduction-effect of the physical vulnerability curve, the standard deviation of yield loss ratio was slightly lower than that of drought hazard intensity index. Here the standard deviation of yield loss ratio for east part was from 0.1 to 0.3. For middle and west part, it was ranging from 0 to 0.2.So the interannual instability of yield loss was reduced. Fig. 11 is the slope of linear regression of yield loss ratio. Slope larger than 0 is showed with warm-toned colors and represents the increasing tendency of yield loss ratio, while slope smaller than 0 is showed with cool-toned colors and represents the decreasing tendency of yield loss ratio. The same increasing tendency like slop of drought hazard intensity index was demenstrated. But impacted by the reduction-effect of the physical vulnerability curve, the rising trend was slightly lower compared with the slope of drought hazard intensity index. Here the highest values of slope of yield loss ratio (exceeding 0.004) centered on middle part, while the other parts changed from 0 to 0.002.

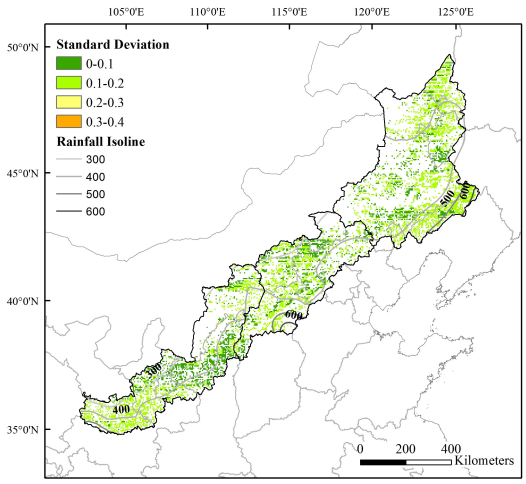

Figure 10: Standard deviation of spring maize yield loss ratio from 1966 to 2011.

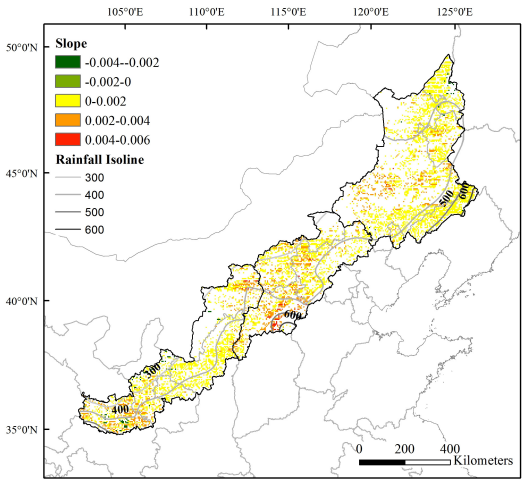

Figure 11: Slope of linear regression of spring maize yield loss ratio from 1966 to 2011.

To assess the risk of yield loss ratio based on physical vulnerability curve in farming-pastoral ecotone in Northern China, we calculated the exceeded probability of yield loss ratio for each evaluation

unit. With fixed yield loss ratio levels (spring maize yield loss ratio≥0.2, spring maize drought yield loss ratio≥0.3, spring maize yield loss ratio≥0.4 and spring maize yield loss ratio≥0.5), the probability distributions of yield loss ratio are shown in Fig. 12. Seen from the whole study area, under different yield loss ratio levels, the middle part and most region of west part were high risk areas of drought hazard with the upper limit of probability under yield loss ratio levels from 0.2 to 0.5 being 1, 1, 0.8 and 0.5 respectively. This meant the drought hazard in these regions would result in yield loss ratio of 0.2 and 0.3 almost every year. And the drought hazard with yield loss ratio of 0.5 would occur at least every two years. Comparatively, the east part within the rainfall isoline from 500mm to 600mm and the southwest edge of the west part was areas with low probability of drought hazard. The upper limit of probability under 4 hazard levels from 0.2 to 0.5 was 0.8, 0.5, 0.2 and 0.2. So this part was more likely to meet drought hazard with yield loss ratio smaller than 0.2. And the probability of drought hazard with yield loss ratio of 0.4 was every five years.

In general, the probability distribution of spring maize yield loss ratio was similar with the probability distribution of drought hazard intensity index. The risk of yield loss ratio dropped from arid to humid region. Because physical vulnerability curves of all three parts showed reduction-effect of drought hazard, the probability of yield loss ratio was slight lower than that of drought hazard intensity index.

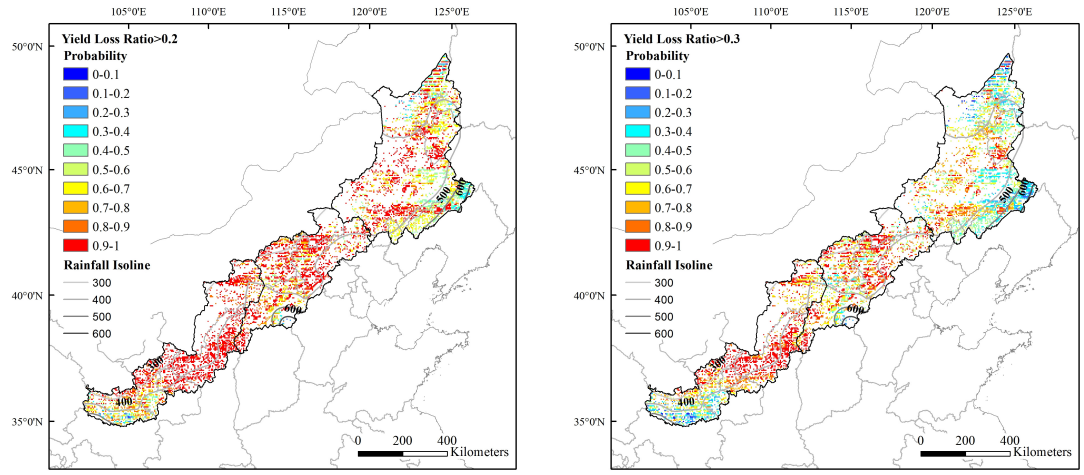

(a) (b)

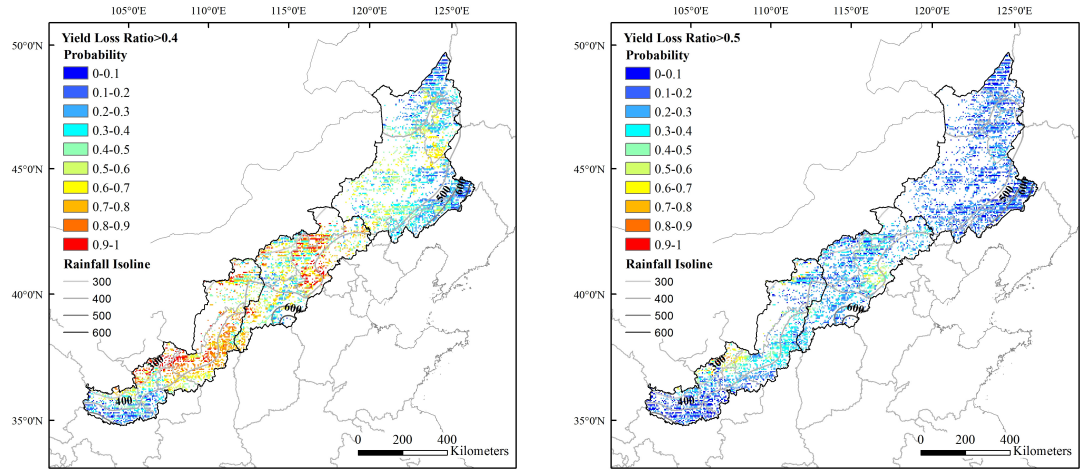

(c) (d)

Figure 12: Probability distribution of spring maize yield loss ratio for different yield loss levels (a) Yield loss ratio≥0.2; (b) Yield loss ratio≥0.3; (c) Yield loss ratio≥0.4; (d) Yield loss ratio ≥0.5.

4 Discussion

Since the disaster risk are the function of hazard factor, physical vulnerability, exposure and the disaster reduction capacity of hazard-affected body, based on the assumption that all maize was exposed to drought hazard, the drought hazard intensity index was calculated through EPIC model and the physical vulnerability curve was established for different parts of farming-pastoral ecotone in Northern China. The risk assessment of drought hazard in study area was discussed from three aspects: The first is the risk assessment of drought hazard intensity index on spring maize. For the spatial distribution of drought hazard intensity index, it had the negative correlation with precipitation. For most years, 400mm rainfall isoline was approximately consistent with drought hazard intensity index of 0.5. For regions with rainfall isoline less than 400mm, drought hazard intensity index here was usually larger than 0.5, while for regions with rainfall isoline higher than 400mm, drought hazard intensity index was usually smaller than 0.5. For the time series of drought hazard intensity index, the time variation of drought hazard intensity index was consistent with the interannual variation of precipitation. For the east part, the interannual variation of precipitation was larger and presented the tendency of worsening drought, so the standard deviation was higher. But for most west part, the situation of drought was relatively stable and the interannual variation of precipitation was smaller, so lower standard deviation of drought hazard intensity index was showed. Also, for most regions in the study area, the drought hazard intensity index presented an increasing tendency throughout years. Drought hazard with sever degree was spreading

from west to northeast in recent years. For the probability of drought hazard intensity index, it showed a tendency of decreasing from southwest to northeast and the tendency of increasing from southeast to northwest alone the distribution of rainfall isoline. The second is the physical vulnerability assessment based on physical vulnerability curve. For three parts of farming-pastoral ecotone in Northern China, similar physical vulnerability curves were got. All of them showed the reduction effect of drought hazard intensity index. The third is the risk assessment of yield loss ratio calculated from physical vulnerability curve. Adjusted by the physical vulnerability curve of spring maize, the fluctuation of yield loss ratio was smaller compared with drought hazard intensity index. Meanwhile, the increasing tendency of yield loss ratio was slowed down and the probability of yield loss ratio was becoming lower. This meant because of the physical vulnerability, the capacity of spring maize to resist and adapt to drought was raised.

The risk assessments showed the farming-pastoral ecotone in Northern China is a region with high risk of agricultural drought and high sensitivity to climate change. Three different parts showed different spatial and temporal distribution of drought hazard intensity index and yield loss ratio. Drought is one of the most manifestations of climate variability in this region and severe droughts are becoming more frequently in recent years. To better adapt to drought, measurements can be taken based on the risk assessment in this study: to reduce the drought hazard intensity, the planting environment can be changed like improving the ability of irrigation or changing soil property through fertilization and other tillage methods. To reduce physical vulnerability of crops to agricultural drought, improved varieties of crops can be developed to promote drought-enduring and drought resisting crops. To reduce crop's exposure to drought, planting structure can be adjusted during the planting process.

The uncertainty of this study mainly comes from the simulation of EPIC model and the construction of physical vulnerability curve. For EPIC model, the uncertainties are from the model itself and input data like meteorological data, soil data and field management data. For the construction of physical vulnerability curve, the uncertainty is mainly due to the limitation of selected sceneries.

The calculation of physical vulnerability curve to agricultural drought proposed in this method provides a probability to assess drought risk quantitatively. Compared with the previous method, a more accurate drought hazard intensity index was added. According to constructive factors of disaster risk, under the condition of total exposure, the risk assessment was conducted from drought hazard intensity index, physical vulnerability and the yield loss ratio calculated from physical vulnerability curve, which gave a synthetically assessment on risk of physical vulnerability to agricultural drought of

farming-pastoral ecotone in Northern China. For the further study, a larger study area including south and north part of China will be selected to better assess drought risk and describe the impact of climate change to agriculture along different latitudes.

5 Conclusion

This study proposed a method to calculate physical vulnerability curve based on the drought hazard intensity index and yield loss ratio from EPIC model. The genetic parameters of spring maize were first calculated according to the statistical yearbook. Then a water-deficit experiment on different growth stage was conducted to get the yield loss contribution rate. And the drought hazard intensity index was calculated from the daily water stress and yield loss contribution rate for different growth stages. After this, the yield loss ratio was got from the difference of yield with two different simulated scenarios with EPIC model (One was sufficient irrigation and the other one was no irrigation). Then sites under different drought hazard intensity were selected. A Logistc model was used to build the relationship between hazard and loss and simulate the physical vulnerability curve. Based on the function of disaster risk, under the condition of totally exposure, the risk assessment of agricultural drought of farming-pastoral ecotone in Northern China was conducted from the drought hazard intensity index and physical vulnerability curve. Seen from drought hazard intensity index, the risk of agricultural drought represented negative correlation with the precipitation. The intensity of drought hazard kept rising for the past 46 years and drought hazard with sever extent was spreading from southwest to northeast gradually. The probability distribution of drought hazard intensity index decreased from southwest to northeast and increased from southeast to northwest alone the rainfall isoline. For the physical vulnerability curve, its reduction effect in three parts of farming-pastoral ecotone in Northern China helped reduce drought hazard vulnerability on spring maize. For the risk of yield loss ratio based on physical vulnerability curve, the probability was lower compared with the drought hazard intensity index which shows the capacity of spring maize to resist drought and its adaptation to drought. Overall, the farming-pastoral ecotone in Northern China is highly sensitive and very fragile to climate change because of its location with several different transitional zones. Risk assessment of physical vulnerability to agricultural drought on this region can help people have a better understanding of physical vulnerability to agricultural drought and can also promote measurements from different fields to adapt to the climate change.

Acknowledgments. This work was supported by a grant entitle ‘‘Study on Agricultural Drought Risk Formation Mechanism of the Rain-fed Agricultural Typical Area in China’’ (41001059) from the National Science and Technology Foundation. We also thank China Meteorological Administration (CMA) for data sharing.

Reference

Alcamo, J., Acosta-Michlik, L., Carius, A., Eierdanz, F., Klein, R., Krömker, D., and Tänzler, D.: A new approach to the assessment of vulnerability to drought, Presented at Concluding Symposium of the German Climate Research Programme (DEKLIM), 2005,

Angstrom, A.: Solar and terrestrial radiation. Report to the international commission for solar research on actinometric investigations of solar and atmospheric radiation., Quarterly Journal of the Royal Meteorological Society, 50, 121-126, 1924.

Antwi-Agyei, P., Fraser, E. D., Dougill, A. J., Stringer, L. C., and Simelton, E.: Mapping the vulnerability of crop production to drought in Ghana using rainfall, yield and socioeconomic data, Applied Geography, 32, 324-334, 2012.

AQSIQ/SAC: GB/T 21986-2008 Assessment of agroclimate impact: Classification method of annual crop climate types. Beijing, General Administration of Quality Supervision, Inspection and Quarantine of the People's Republic of China/Standardization Administration of the Peoples Republic of China. In Chinese., 2008.

Azadi, H., van den Berg, J., Shahvali, M., and Hosseininia, G.: Sustainable rangeland management using fuzzy logic: A case study in Southwest Iran, Agriculture, ecosystems & environment, 131, 193-200, 2009.

Blaikie, P. C., and Cannon, T.: At Risk, natural hazards, people’s vulnerability and disasters, Disaster and society from hazard assessment to risk reduction, Berlin, 75-82, 1994.

Douglas, J.: Physical vulnerability modelling in natural hazard risk assessment, Natural Hazards and Earth System Science, 7, 283-288, 2007.

Füssel, H.-M.: Vulnerability: a generally applicable conceptual framework for climate change research, Global Environmental Change, 17, 155-167, 2007.

FAO: The State of Food Insecurity in the World 2001. The multiple dimensions of food security. Rome., 2001.

FAO, I. a. W.: The State of Food Insecurity in the World 2013. The multiple dimensions of food security. Rome., 2013.

Gassman, Philip Walter Williams, Jimmy R Benson, Verel W Izaurralde, R César Hauck, Larry M Jones, C Allan Atwood, Jay D Kiniry, James R Flowers, and D, J.: Historical development and applications of the EPIC and APEX models, Center for Agricultural and Rural Development, Iowa State University, 2005.

Geng, Q., Wu, P., Zhang, Q., Zhao, X., and Wang, Y.: Dry/wet climate zoning and delimitation of arid areas of Northwest China based on a data-driven fashion, Journal of Arid Land, 6, 287-299, 2014.

Herrmann, S. M., Anyamba, A., and Tucker, C. J.: Recent trends in vegetation dynamics in the African Sahel and their relationship to climate, Global Environmental Change, 15, 394-404, 2005.

Hufkens, K., Scheunders, P., and Ceulemans, R.: Ecotones in vegetation ecology: methodologies and definitions revisited, Ecological Research, 24, 977-986, 2009.

IPCC: Climate Change 2014: Synthesis Report. Contribution of Working Groups I, II and III to the Fifth Assessment Report of the Intergovernmental Panel on Climate Change, 2014.

Izaurralde, R. C., Mcgill, W. B., and Williams, J.: Development and application of the EPIC model for carbon cycle, greenhouse-gas mitigation, and biofuel studies, Pacific Northwest National Laboratory (PNNL), Richland, WA (US), 2012.

Jain, V., Pandey, R. P., and Jain, M.: Spatio-temporal assessment of vulnerability to drought, Natural Hazards, 76, 443-469, 10.1007/s11069-014-1502-z, 2015.

Jia, H., Wang, J., Cao, C., Pan, D., and Shi, P.: Maize drought disaster risk assessment of China based on EPIC model, International Journal of Digital Earth, 5, 488-515, 2012.

Karavitis, C. A., Tsesmelis, D. E., Skondras, N. A., Stamatakos, D., Alexandris, S., Fassouli, V., Vasilakou, C. G., Oikonomou, P. D., Gregorič, G., and Grigg, N. S.: Linking drought characteristics to impacts on a spatial and temporal scale, Water Policy, 16, 1172-1197, 2014.

Kark, S.: Ecotones and ecological gradients, in: Ecological Systems, Springer, 147-160, 2013.

Kellner, O., and Niyogi, D.: FORAGES AND PASTURES SYMPOSIUM: Assessing drought vulnerability of agricultural production systems in context of the 2012 drought, Journal of animal science, 92, 2811-2822, 2014.

Kim, H., Park, J., Yoo, J., and Kim, T.-W.: Assessment of drought hazard, vulnerability, and risk: A case study for administrative districts in South Korea, Journal of Hydro-environment Research, 2013.

Kim, H., Park, J., Yoo, J., and Kim, T.-W.: Assessment of drought hazard, vulnerability, and risk: a case study for administrative districts in South Korea, Journal of Hydro-environment Research, 9, 28-35, 2015.

Liu, J.-h., Gao, J.-x., Lv, S.-H., Han, Y.-w., and Nie, Y.-h.: Shifting farming–pastoral ecotone in China under climate and land use changes., Journal of arid environments, 75, 298-308, 2011.

Lu, W., and Jia, G.: Fluctuation of farming-pastoral ecotone in association with changing East Asia monsoon climate, Climatic change, 119, 747-760, 2013.

Murthy, C., Yadav, M., Ahamed, J. M., Laxman, B., Prawasi, R., Sai, M. S., and Hooda, R.: A study on agricultural drought vulnerability at disaggregated level in a highly irrigated and intensely cropped state of India, Environmental monitoring and assessment, 187, 1-14, 2015.

Piao, S., Ciais, P., Huang, Y., Shen, Z., Peng, S., Li, J., Zhou, L., Liu, H., Ma, Y., and Ding, Y.: The impacts of climate change on water resources and agriculture in China, Nature, 467, 43-51, 2010.

Prescott, J.: Evaporation from a water surface in relation to solar radiation., Transactions of the Royal Society of South Australia, 64, 114-118, 1940.

Pumijumnong, N., and Arunrat, N.: Simulating the rice yield change in Thailand under SRES A2 and B2 scenarios with the EPIC model, Journal of Agri-Food and Applied Sciences, 1, 119-125, 2013.

Rian, S., Xue, Y., MacDonald, G. M., Touré, M. B., Yu, Y., De Sales, F., Levine, P. A., Doumbia, S., and Taylor, C. E.: Analysis of climate and vegetation characteristics along the Savanna-Desert ecotone in Mali using MODIS data, GIScience & Remote Sensing, 46, 424-450, 2009.

Rinaldi, M., and De Luca, D.: Application of EPIC model to assess climate change impact on sorghum in southern Italy, Italian Journal of Agronomy, 7, 12, 2012.

Sharma, U., and Patwardhan, A.: Methodology for identifying vulnerability hotspots to tropical cyclone hazard in India, Mitigation and Adaptation Strategies for Global Change, 13, 703-717, 2008.

Shi, W., Tao, F., Liu, J., Xu, X., Kuang, W., Dong, J., and Shi, X.: Has climate change driven

spatio-temporal changes of cropland in northern China since the 1970s?, Climatic change, 124, 163-177, 2014.

Simelton, E., Fraser, E. D., Termansen, M., Forster, P. M., and Dougill, A. J.: Typologies of crop-drought vulnerability: an empirical analysis of the socio-economic factors that influence the sensitivity and resilience to drought of three major food crops in China (1961–2001), Environmental Science & Policy, 12, 438-452, 2009.

Skaggs, T., Arya, L., Shouse, P., and Mohanty, B.: Estimating particle-size distribution from limited soil texture data, Soil Sci. Soc. Am. J., 65, 1038-1044, 2001.

UNDP: Reducing Disaster Risk: A Challenge for Development-a Global Report, United Nations Development Programme, 2004.

UNISDR Terminology on Disaster Risk Reduction: https://www.unisdr.org/we/inform/terminology, 2009.

Uzielli, M., Nadim, F., Lacasse, S., and Kaynia, A. M.: A conceptual framework for quantitative estimation of physical vulnerability to landslides, Engineering Geology, 102, 251-256, 2008.

Wang, Z., He, F., Fang, W., and Liao, Y.: Assessment of physical vulnerability to agricultural drought in China, Nat. Hazards, 67, 645-657, 2013a.

Wang, Z., He, F., Fang, W., and Liao, Y.: Assessment of physical vulnerability to agricultural drought in China., Natural hazards, 67, 645-657, 2013b.

Wang, Z., Jiang, J., Liao, Y., and Deng, L.: Risk assessment of maize drought hazard in the middle region of farming-pastoral ecotone in Northern China, Natural Hazards, 76, 1515-1534, 2015.

Wheeler, T., and von Braun, J.: Climate change impacts on global food security, Science, 341, 508-513, 2013.

Xiong, W., Balkovič, J., van der Velde, M., Zhang, X., Izaurralde, R. C., Skalský, R., Lin, E., Mueller, N., and Obersteiner, M.: A calibration procedure to improve global rice yield simulations with EPIC, Ecological Modelling, 273, 128-139, 2014.

Xu, D., Li, C., Song, X., and Ren, H.: The dynamics of desertification in the farming-pastoral region of North China over the past 10years and their relationship to climate change and human activity, CATENA, 123, 11-22, 2014.

Ye, Y., and Fang, X.: Boundary shift of potential suitable agricultural area in farming-grazing transitional zone in Northeastern China under background of climate change during 20th century, Chinese Geographical Science, 23, 655-665, 2013.

Zhao, H., Zhao, X., Zhang, T., and Zhou, R.: Boundary line on agro-pasture zigzag zone in north china and its problems on eco-environment., Advance in earth sciences, 17, 739-747 (In Chinese), 2002.

Zou, X., Zhai, P., and Zhang, Q.: Variations in droughts over China: 1951–2003, Geophysical Research Letters, 32, 2005.